Strain determination in multilayers by complementary anomalous x-ray diffraction

T. U. Schülli,[1,2] R. T. Lechner,[1] J. Stangl,[1] G. Springholz,[1] G. Bauer,[1] M. Sztucki,[2] and T. H. Metzger[2]
[1]*Institute for Semiconductor Physics, Johannes Kepler Universität Linz, A-4040 Linz, Austria*
[2]*European Synchrotron Radiation Facility, BP 220, F-38043 Grenoble Cedex, France*
(Received 19 November 2003; revised manuscript received 24 February 2004; published 20 May 2004)

A method to determine selectively the lattice parameters and the strain in multilayers is developed, based on x-ray diffraction, using two wavelengths close to the absorption edges of different elements. This allows for a complementary suppression of the constituent materials in the multilayer. The method is applied to a study of single crystal multilayers of EuSe and PbSeTe grown by solid source molecular-beam epitaxy. The enhancement of the chemical contrast by anomalous x-ray diffraction and the high resolution is exploited to achieve a sensitivity for interdiffusion on an angstrom scale.

DOI: 10.1103/PhysRevB.69.195307 PACS number(s): 68.65.−k, 61.10.Eq

I. INTRODUCTION

Strain and interdiffusion in multilayered semiconductor devices are crucial features for their functionality. The band structure as well as the two-dimensional confinement effects are determined by these properties. In heteroepitaxial structures, x-ray diffraction is usually the tool of choice to determine lattice parameters and hence strain. In the case of overlapping intensities from similar lattice parameters of two distinct materials, and especially, if interdiffusion between the materials can occur, the precise determination of their strain state and a discrimination between strain and composition remains ambiguous to a certain extent. Indirect methods based on elaborate fitting of the diffraction patterns are usually applied for the analysis.[1–3]

We present here a method based on anomalous diffraction, i.e., the tuning of x-ray energies close to absorption edges of the constituent elements of multilayers. The method can be employed for all compound materials with superstructure reflections, such as the zincblende or the rock salt structure. Using two distinct x-ray energies, the scattering contribution from one material can be greatly reduced compared to a second one, and vice versa. Fitting the scattering spectra obtained at the two energies with a single set of parameters considerably enhances the sensitivity to strain, and allows for a clear discrimination of strain and composition. As the analysis requires the tuning of x-ray energy, measurements need to be performed at a synchrotron source. As a model system to demonstrate the method, we study lead and europium chalcogenides for two reasons. First, Eu compounds exhibit magnetic properties which depend sensitively on lattice strain.[4,5] Second, these compounds offer strong anomalous scattering, which allows for a clear presentation of the method.

The combination of PbSe and EuSe in heterostructures and multilayers promises a tuning of the magnetic and optical properties of EuSe.[6] Neutron-scattering experiments from bulk EuSe under high hydrostatic pressure have shown that a change in the lattice parameter drastically influences the magnetic exchange interaction between the Eu ions.[4] The biaxial stress in pseudomorphic heteroepitaxial multilayers has a similar effect.[5,7] EuSe has a cubic lattice parameter of $a_{\mathrm{EuSe}}=6.187$ Å, the lattice parameter of PbSe and PbTe are $a_{\mathrm{PbSe}}=6.124$ Å and $a_{\mathrm{PbTe}}=6.462$ Å, respectively. Changing the ternary composition in EuSe/$\mathrm{PbSe}_{(1-x)}\mathrm{Te}_x$ ($x=0$–0.4) multilayers, a change of the EuSe in-plane lattice parameter by -1.0 to $+1.2\%$ corresponding to a distortion in growth direction between $+0.75\%$ and -0.83% can be achieved for perfect pseudomorphic growth. It is therefore of special interest to selectively determine the strain in EuSe with a precision of 0.1% of the lattice parameter. Due to the similarity of the lattice parameters of the two epilayers and the usually much larger thickness of the $\mathrm{PbSe}_{(1-x)}\mathrm{Te}_x$ spacer layers together with Pb as the strongest x-ray scatterer, it is difficult to extract detailed strain information about the EuSe layers from a conventional high-resolution diffraction pattern.

In Sec. II, the selective suppression of scattering from a particular binary material is explained in detail. Section III describes the anomalous diffraction experiments on EuSe/PbSe multilayers. The results are discussed in Sec. IV. The numerical simulation of scattering patterns is summarized in the Appendix.

II. SUPPRESSION OF A BRAGG REFLECTION

Anomalous scattering can be employed to suppress superstructure reflections in compound crystals.[8] Our model system crystallizes in the rock salt structure. Here the scattering amplitude from, e.g., the (111) reflection in PbSe reads $F_{(111)}=4(f_{\mathrm{Pb}}-f_{\mathrm{Se}})$, and accordingly for the other binary compounds. The atomic scattering factors f_{Pb}, f_{Eu}, f_{Se}, and f_{Te} are complex numbers composed of a momentum dependent part f_0 and resonant corrections f' and $i\times f''$ depending on x-ray energy: $f(\mathbf{q},E)=f_0(\mathbf{q})+f'(E)+if''(E)$. For certain energies and momentum transfers $\mathbf{q}$, the scattering factors of two elements can become equal, and consequently, the scattering amplitude of the corresponding compound vanishes.

The momentum dependence of f_0 can be calculated for all elements according to the parametrization published in Ref. 9. f' and f'' are generally taken from international tables.[10,11] Close to absorption edges, however, an experimental determination of the scattering factors is necessary, as the exact location of the edges as well as the variation of f' and f'' in the vicinity of absorption edges can deviate from the theoretical values. Additionally, such a measurement already in-

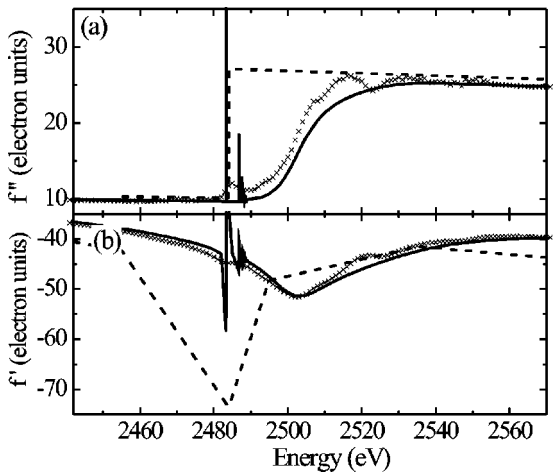

FIG. 1. (a) Values of f'' for Pb in the vicinity of the Pb M_V edge as determined by fluorescence measurements (crosses), compared to values from different international tables (dashed and full lines). (b) Evolution of f' for Pb in the same energy regime as in (a).

cludes the energy resolution of the experimental setup in the determined values of f' and f'' that are later used to simulate the diffraction spectra.

Usually f'' is measured by absorption. At low x-ray energies and for heavy elements as Pb, this would require an extremely thin foil. It is therefore easier to measure the fluorescence yield from a thin film as a proportional measure of absorption. For our calibration, a 100 nm thick PbSe film was irradiated with x rays and the Pb fluorescence was recorded as a function of the incident x-ray energy across the Pb M_V edge. With the tables given in Ref. 12, based on Ref. 11, the values for f'' were extrapolated up to 250 keV and f' was calculated for Pb via the Kramers-Kronig relation. The measured and calculated values of f'' and f' are plotted as crosses in Figs. 1(a) and 1(b) as a function of energy.

In the case of the Pb M_V edge, we observed a significant deviation of the edge energy from the tabulated values that are generally used. In the international tables based on Refs. 10 and 11, the Pb M_V-edge value is given as 2484 eV, whereas we determined a value of 2502 eV. However, the evolution of f'' in the vicinity of the Pb M_V edge in our measurement coincides well with the values given in Ref. 12. For comparison, the values according to Refs. 10 (dashed line) and 12 (based on Ref. 11; full line) are added. The latter are in good agreement with our experimental results.

The real parts of the complex atomic form factors of the four concerned elements, as well as the calculated and measured evolution of the (111) Bragg intensity from PbSe and PbTe are plotted in Fig. 2 as a function of energy. As Pb (82 electrons) is much heavier than Se (34 electrons) and Te (52 electrons), it is not possible to achieve $f_{\mathrm{Pb}}=f_{\mathrm{Se}}$ or $f_{\mathrm{Pb}}=f_{\mathrm{Te}}$ at the K or L edges of Pb. Close to the Pb M_V edge around 2500 eV, however, the resonance causes a decay of the atomic form factor of Pb down to an intersection point with the Te and even the Se form factor, resulting in a strong suppression of the PbSe or PbTe (111) reflection at these intersection energies, as shown in detail in Fig. 2(b). For any

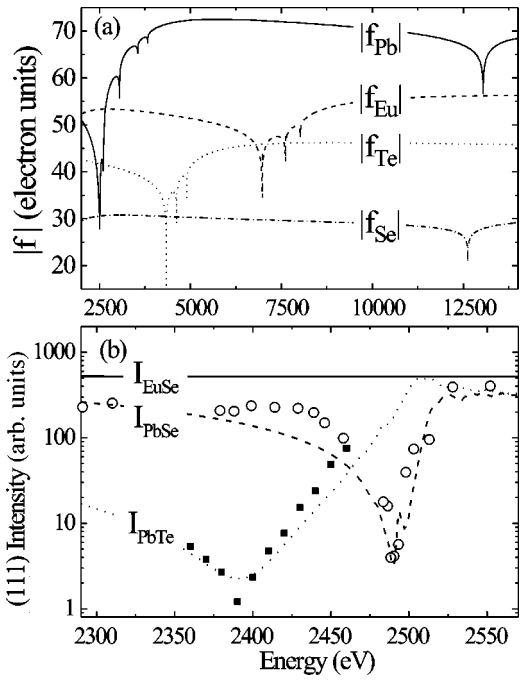

FIG. 2. (a) Absolute values of $|f_{Pb}|$ (full line), $|f_{Eu}|$ (dashed), $|f_{Te}|$ (dotted), and $|f_{Se}|$ (dash dotted) according to Ref. 12 and for a momentum transfer of $q=1.75$ Å^{-1}, corresponding approximately to the PbSe and EuSe (111) Bragg reflections. (b) Calculated (111) Bragg intensity from EuSe (full line), PbSe (dashed), and PbTe (dotted) in the vicinity of the Pb M_V edge. The diffracted intensities as measured are added as for PbTe (full squares) and PbSe (open circles).

ternary alloy $PbSe_{(1-x)}Te_x$ the intersection energy lies in between. For f_{Eu} and f_{Se}, there exists no intersection point in the x-ray regime, however, a significant minimum in the intensity of the EuSe (111) reflection occurs below the Eu L_{III} edge at 6977 eV.

III. EXPERIMENTS

All diffraction experiments were carried out in specular reflectivity geometry, up to scattering angles of 140°. This high angular range was required in order to achieve the necessary momentum transfers at x-ray energies as low as 2500 eV. We have recorded line scans along **q** across the specular (111) Bragg reflection of EuSe/PbSe and EuSe/$PbSe_{(1-x)}Te_x$ multilayer superlattices grown in ⟨111⟩ direction by solid source molecular-beam epitaxy (MBE) onto BaF_2(111) single-crystal substrates. Details about the MBE growth will be published elsewhere.[13] The thicknesses of the superlattice layers, the number of bilayers as well as the Te content x in the ternary layers of the three investigated samples are listed in Table I.

Since x-ray energies below 4 keV are required, where air and almost any other material show strong x-ray absorption, we used an in-vacuum diffractometer with windowless operation at the beamline ID01 at the ESRF in Grenoble. To perform diffraction experiments at x-ray energies around 2.5 keV remains an experimental challenge but offers resolution

TABLE I. Growth parameters of the investigated multilayers. The thicknesses of the epilayers as deposited in the MBE process are given in angstrom. In addition, the number of bilayers and the Te content x in $PbSe_{1-x}Te_x$ are given.

Sample	M1420	M1553	M1555
T (°C)	380	230	260
d_{EuSe} (Å)	36	45	45
$d_{PbSe_{1-x}Te_x}$ (Å)	64	440	288
Number of periods	30	100	100
x	0	0	0.1

benefits, since the coherence length of the x-rays scales with the wavelength. This is of particular importance in the case of high-quality multilayers. For a sample with a total thickness of about 0.3 μm, the whole multilayer stack can be coherently illuminated at 2490 eV, but not at e.g., 12 300 eV, which is a typical energy usually exploited in diffraction. For both cases, radial scans along **q** across the specular (111) reflection were measured, which are plotted in Figs. 3(a) and 3(b), together with simulations. For clarity, the simulations are shifted downwards with respect to the measurement.

For all x-ray energies, the same collimation settings were used, leading to a similar photon flux. The perfection of growth is visible only at 2490 eV in Fig. 3(a). In this case, all $(N-2)=28$ side maxima of the interference function of the 30 bilayers are visible, proving a coherent growth of the crystal lattice throughout the complete multilayer. In the measurement at 12 300 eV, the oscillations are smeared out, hence the data do not allow for an equally detailed analysis.

IV. DISCUSSION

A. Perfect multilayers

For a heteroepitaxial $EuSe/PbSe_{(1-x)}Te_x$ multilayer, it is possible to choose two complementary energies, pronouncing either the EuSe or the $PbSe_{(1-x)}Te_x$ scattering, and suppressing the other component, as shown for sample M1420 in Fig. 3, together with simulations. All simulations are performed for perfect growth and take into account the energy dependent anomalous dispersion. They are convoluted with the resolution function of the experiment, which depends on the wavelength, the collimation conditions and the incident and exit angles of the x-ray beam. To the left and to the right of the highest multilayer satellite peak, the (111) Bragg peaks of the BaF_2 substrate ($a_{BaF_2}=6.200$ Å) and the 2.3 μm thick PbSe buffer layer are visible, indicated by vertical lines in Figs. 3(a) and 3(b). Their influence on the diffraction pattern is certainly more important in the case of the data recorded at higher x-ray energy in Fig. 3(b). The reason is the strong suppression of the PbSe scattering at 2490 eV by a factor of 400 with respect to 12 300 eV. Additionally, the high absorption at low x-ray energies leads to a significant weakening of the substrate reflection, being covered by 2.6 μm of material. This is a considerable advantage for quantitative data analysis.

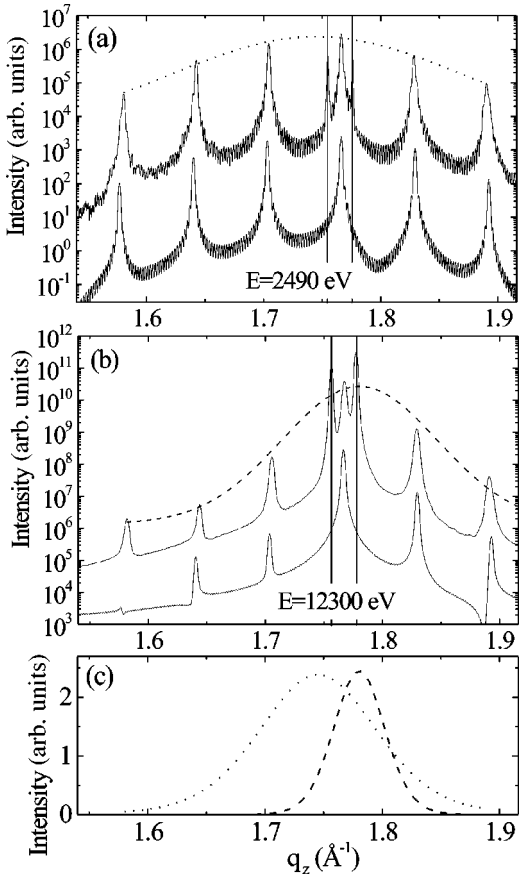

FIG. 3. (a) Radial scan across a multilayer of 30×64 Å PbSe/36 Å EuSe (sample M1420) with an x-ray energy of 2490 eV. The simulation (lower line plot) is shifted with respect to the experiment for clarity. The dotted line represents Gaussian fit to the envelope of the satellite peaks. (b) Corresponding scan to (a) but at an x-ray energy of 12 300 eV. Vertical lines in (a) and (b) mark the positions of the Bragg peaks from the BaF_2 substrate and the 2 μm PbSe buffer layer. (c) The plots of the fitted envelopes from (a) and (b) on a linear scale for comparison.

For the measurements on the multilayer presented in Figs. 3(a) and 3(b), the strain for both materials in the multilayer can be obtained via a direct method. In the case of a perfect multilayer with well-defined thicknesses of the single layers, the width of the envelope of the satellite reflections carries the information about the thickness of a single bilayer. Its position supplies, as explained in the following, the distance of the (111) lattice planes. This distance is also referred to as the (111) d spacing. In the kinematic description of the multilayer diffraction given in detail in the Appendix, the specular reflectivity amplitude is expressed by the summation over all multilayer periods N (i.e., the total number of bilayers)

$$A(q)=\sum_{l=1}^{N} e^{iql(M_{EuSe}d_{111_{EuSe}}+M_{PbSe}d_{111_{PbSe}})}[\mathrm{FT}\{\mathrm{bilayer}\}]. \tag{1}$$

With M_{EuSe} as the number of atomic monolayers and $d_{111_{EuSe}}$ as the d spacing of the EuSe (111) planes, $M_{EuSe}d_{111_{EuSe}}$ cor-

responds to the thickness of the EuSe film and the equivalent description to the thickness of the PbSe film that form the bilayer. In Eq. (1), the sum in the first line describes the geometrical factor giving rise to the satellite maxima. It corresponds to the grating interference function known from optics textbooks.[14] The expression in brackets in the second line describes the Fourier transform of the bilayer and hence simply envelopes the interference function. If the number of bilayers is large, i.e., if the total thickness of the multilayer is large compared to the thickness of one bilayer, the width of the interference satellites is small compared to the width of the envelope. We can then directly use a fitting model of a single bilayer to describe the envelope of our recorded satellites in the data. These considerations can also be derived from the convolution theorem for Fourier transforms (see for instance, Ref. 15).

For 2490 eV, the scattering of EuSe at the (111) reflection is 100 times larger than to that of PbSe, hence the envelope is considered to represent only the scattering from the EuSe layers. At 12 300 eV, the PbSe scattering intensity dominates over the EuSe by a factor of 2.5. As the thickness ratio of the layers of PbSe and EuSe is about 2.0, the scattered intensity at the (111) reflection at 12 300 eV is roughly ten times stronger from the PbSe than from the EuSe layers. Thus the scattering from the EuSe layers is strongly suppressed compared to the experiments for an energy of 2490 eV. Gaussian fits to the envelopes of the superlattice peaks are shown in Fig. 3(c). Their center position corresponds to the reciprocal lattice parameter along growth direction of the layer with stronger scattering intensity. The center lies at 1.74 $Å^{-1}$ for 2490 eV, and at 1.78 $Å^{-1}$ for 12 300 eV, corresponding to a EuSe (111) *d* spacing of 3.61 Å and a PbSe (111) *d* spacing of 3.53 Å. The respective cubic lattice parameters along growth direction are 6.25 Å for EuSe, and 6.11 Å for PbSe. For PbSe, the uncertainty of the lattice parameter is larger due to the disturbing influence of the reflections from substrate and buffer, which still dominate the diffraction pattern in Fig. 3(b). This effect is less perturbing for the other two samples with thicker multilayers, as absorption inside the multilayers weakens these contributions.

B. Imperfect multilayers

As mentioned before, the lattice mismatch between PbSe and EuSe leads to an epitaxial strain in multilayers. To enhance the influence of the PbSe lattice parameter on the in-plane lattice parameter in a coherent EuSe/PbSe multilayer, a thickness ratio of the EuSe and PbSe layers of about 1:10 was chosen for samples M1553 and M1555. In this case the PbSe (111) reflection remains visible in the envelope of the bilayer even at 2490 eV. Despite the fact that the scattering of PbSe is about 100 times weaker than the EuSe scattering, the diffracted intensity at the (111) Bragg position of this multilayer is expected to be of the same order of magnitude for both compounds. As it is proportional to the square of the number of coherent scatterers, the larger thickness of the PbSe layers compensates for their weak structure amplitude. For the thinner EuSe layers we expect a much broader envelope in reciprocal space, therefore both contributions can be easily identified correctly. In the case of a multilayer of 100×440 Å PbSe/ 45 Å EuSe, the (111) reflections from the underlying buffer and substrate will not be visible anymore due to absorption in the multilayer. Another effect might, however, disturb the data evaluation from such thick epitaxial structures. Instabilities in the material flux rates during the long growth procedure will lead to a drift in the thickness of the single layers. The coherent growth of the crystal lattice remains unaffected by this deviation, but the varying bilayer thickness throughout the multilayer leads to a varying phase shift of the bilayers. In reciprocal space, this phase shift is of the order of an integer multiple of the reciprocal (111) *d* spacings. It has therefore almost no effect on the satellite peaks that are located in the vicinity of Bragg positions. The satellites that modulate the Bragg reflection will, however, broaden or split more and more with increasing distance from the Bragg position. The envelope of the superlattice peaks will hence be deformed if only the satellite heights are considered, and the direct evaluation of the lattice parameter via a fit to the envelope can no longer be applied. This effect has already been described for a random variation of the multilayer period in the one dimensional paracrystal model of Hosemann.[16] The variations for epitaxial structures are, however, rather drifts in the growth conditions than random variations.

In a first fitting approach to such structures, it is therefore helpful to convolute data and fitting model with a Gaussian of a width that automatically integrates over the splitted/broadened peaks. This procedure is hence equivalent to fitting the integrated peak intensities. The information that is lost by this convolution is attributed to deviations in the multilayer period. Due to the thickness ratio of the EuSe/PbSe bilayers, the spacing of the satellite reflections is about ten times smaller than the width of the EuSe (111) reflection. A convolution that washes out the splitting of the superlattice satellites will therefore neither affect the width nor the position of the EuSe envelope significantly. Figure 4(a) shows the diffraction pattern of this superlattice recorded at 2490 eV as a full black line. The Gaussian that was used to convolute data and simulation had a width of 0.01 $Å^{-1}$ and is plotted on the left side as a dashed line. To ensure that the convolution does not disturb the analysis of the lattice parameter, the width of this Gaussian is narrower than the expected one of the PbSe envelope of $2\pi/440$ $Å^{-1}$ $=0.0143$ $Å^{-1}$ and significantly narrower than that of EuSe with an expected width of $2\pi/45$ $Å^{-1}=0.14$ $Å^{-1}$. The convolution reproduces the envelope function expected for a perfect multilayer. The EuSe lattice constant can be determined regardless of whether or not the fitting model describes the thickness variations in the multilayer correctly. The convoluted data are plotted in Fig. 4(a) as circles, together with the convoluted fit (full line).

The resulting EuSe (111) *d* spacing is 3.60 Å corresponding to a cubic lattice parameter of 6.23 Å, for PbSe a lattice parameter in growth direction of 6.123 Å is obtained. To illustrate the resolution of this method, a simulation for a EuSe lattice parameter of 6.26 Å is plotted as well (dash-dotted line). The scattering pattern is already significantly different from the best fit. Figure 4(b) shows the simulation

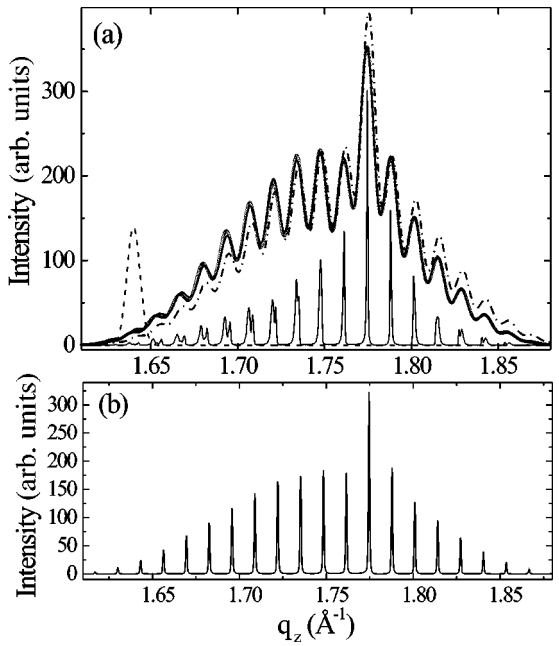

FIG. 4. (a) Scan across the (111) reflection of a 100×440 Å PbSe/ 45 Å EuSe multilayer (lower full black line) and its convolution (circles) with a Gaussian of 0.01 Å^{-1} width (dashed line). The best fit of the simulation convoluted with the same Gaussian is plotted as a full line. The dash-dotted line represents a deviation of the EuSe lattice parameter by 0.5% of the best fit for comparison. (b) Simulation of the perfect multilayer without convolution.

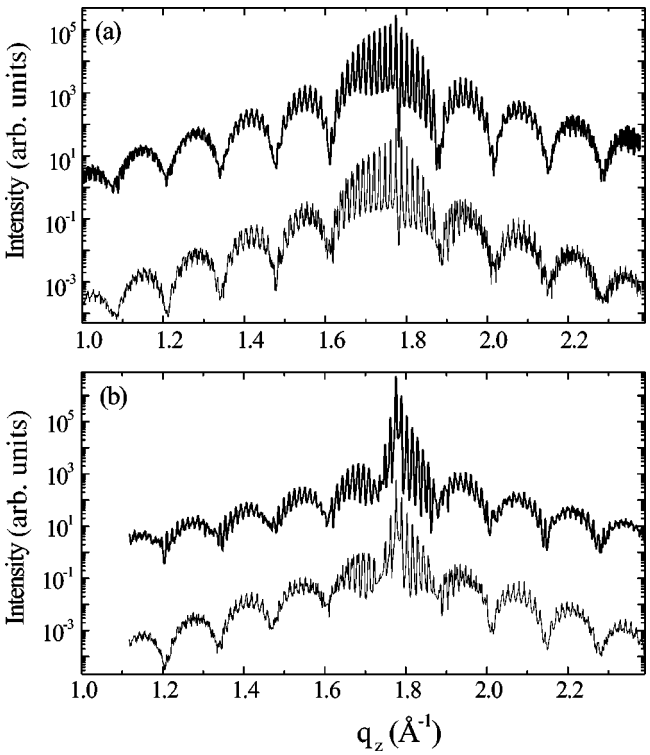

FIG. 5. Scans across the (111) reflection of a 100×440 Å PbSe/ 45 Å EuSe multilayer [lower line plots in (a) and (b)] at 2490 eV in (a) and 6975 eV in (b). The line plots shifted towards higher intensity represent the best-fit simulations.

of the same multilayer diffraction pattern with the same strain situation as the best fit in (a), but without taking into account any deviations of the bilayer periodicity and without the convolution. It is clearly visible that the envelope in (b) is different from that of the recorded raw data in (a), but can be recovered when the integrated intensity of the satellites is considered.

With the parameters for the strain state of the layers derived by this method we can proceed with a more elaborate simulation to describe the diffraction spectra of the sample and include imperfections to the multilayer periodicity. Choosing appropriate x-ray energies, we obtain complementary sensitivity to either the PbSe or the EuSe layers: Two spectra were recorded over a wide range across the (111) reflection for 2490 eV (PbSe suppression) and 6975 eV (EuSe suppression). These scans are plotted in Figs. 5(a) and 5(b) (lower plots in the graphs). Their best fits are added and shifted for clarity. Both scans were fitted with an *ab initio* description of the whole multilayer as a linear stack of atoms. This numerical procedure allows for an easy handling of imperfections such as a drift in the layer thicknesses and interdiffusion. Monoatomic steps that are known to exist on the cleaved substrate and which reproduce in layer-by-layer growth[7] are also taken into account. These steps can be treated as a roughness on a large lateral lengthscale and become important if the lateral coherence length of the x-ray beam on the surface exceeds the average distance between two steps. For the low x-ray energies used here, this is the case. Interdiffusion and roughness on a short lengthscale are not discriminated in the model and are taken into account by averaging the atomic scattering factors in the vicinity of the interface. The monoatomic steps lead to phase shifts between large areas of the superlattice and hence lead to interference phenomena that decrease the intensity on the truncation rod.[17]

The scans in Fig. 5 carry complementary information on the strain in both materials and lead to a refinement of the input parameters gained from the procedure presented in Fig. 4. The corresponding cubic lattice parameter for PbSe in growth direction is determined to be 6.115 Å, the value for EuSe remains unchanged at 6.23 Å. Taking into consideration the elastic properties of PbSe and EuSe, one can calculate the theoretical in-plane values for the lattice parameters. This results in 6.132 Å for PbSe and 6.13 Å for EuSe, which is in agreement with the expected pseudomorphic growth of the superlattice stack, if we use previously published elastic constants of the constituent materials.[6,18]

The uniaxial expansion or compression into growth direction of the magnetic EuSe layers can be tuned by a change of the lattice constant of the spacer layers. Assuming pseudomorphic growth in the plane, the latter represents a boundary condition that provokes as a response the strain in growth direction. In the systems investigated here, the in-plane lattice constant is controlled by substitution of a part of the Se by Te in the PbSe spacers. A multilayer of 100 ×[288 Å $PbSe_{0.9}Te_{0.1}$/45 Å EuSe] was grown in order to reduce the lattice mismatch between both materials to 0.5%. The complementary diffraction patterns were recorded at

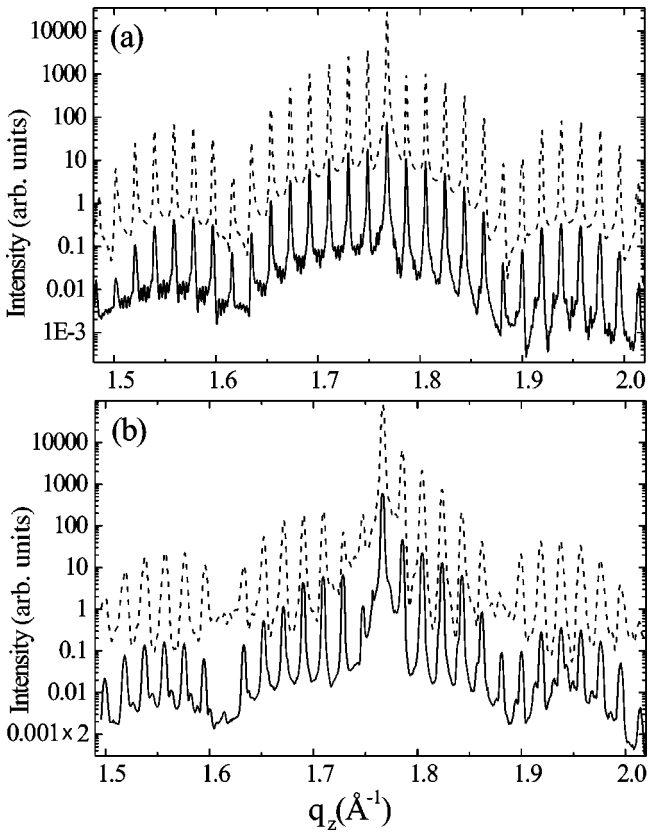

FIG. 6. Scans across the (111) reflection of a 100 $\times$288 Å $PbSe_{0.9}Te_{0.1}$/ 45 Å EuSe multilayer [full lines in (a) and (b)] at 2475 eV in (a) and 6975 eV in (b). The dashed lines represent the best fit simulations that are shifted towards higher intensity.

2475 eV ($PbSe_{0.9}Te_{0.1}$ suppression) and at 6975 eV (EuSe suppression) and are plotted in Fig. 6. As for Fig. 5, the best-fit simulations are added.

C. Determination of interdiffusion

An important parameter that can be extracted from the fits in Fig. 5 is the interdiffusion at the interfaces. Recording the scattered x-ray intensity along the crystal truncation rod is known to be a tool for the investigation of roughness at surfaces and interfaces.[17,19–21] In our case, the strong scattering contrast leads to a particular sensitivity for the chemical composition. The numerical modeling of the diffraction spectra was performed via averaging the atomic form factors across the interface, as described in detail in the Appendix. To compare the results for the interdiffusion decay, we define the interdiffusion length μ as the length over which the concentration of one compound has changed from 25% to 75%. The result of the best fit proves an extremely well-defined interface with an interdiffusion decay length μ of only 1.0 Å, much less than the thickness of one PbSe (440 Å) or EuSe (45 Å) layer. To demonstrate the sensitivity to this parameter, simulations for two different interdiffusion lengths are shown in Fig. 7(a) together with the recorded data at 2490 eV. The red line represents the best fit, with an interdiffusion length of $\mu = 1.0$ Å, the blue line corresponds to an interdiffusion

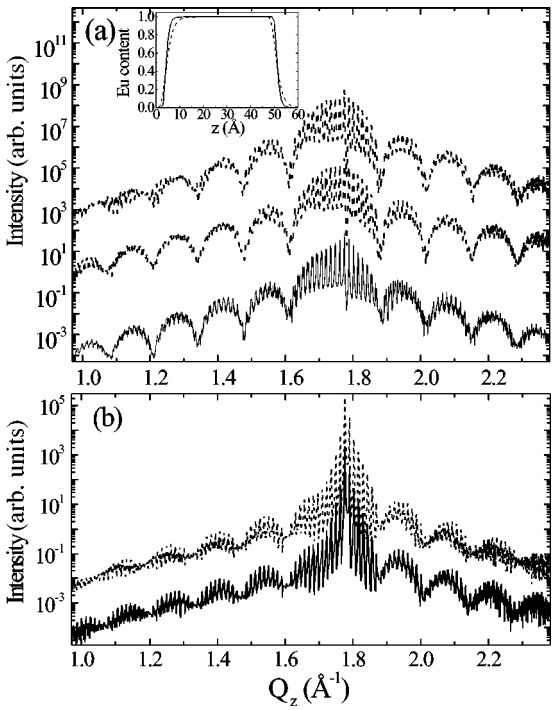

FIG. 7. Influence of interdiffusion on the modulation along the truncation rod. (a) The scan recorded at 2490 eV across the (111) reflection is plotted as a full line. The best-fit simulation (lower dashed plot) corresponds to an interdiffusion length of 1.0 Å, the uppermost dashed plot refers to 2.0 Å. The EuSe concentration profiles for both simulations are shown in the inset (full line for 1.0 Å, dashed line for 2.0 Å). (b) Two simulations for the same interdiffusion profiles as in (a) but for an x-ray energy of 8050 eV. The full line for an interdiffusion length of 1.0 Å, the dashed one to 2.0 Å.

length of $\mu = 2.0$ Å. The thin film Laue oscillations of the envelope are clearly less pronounced in the case of the blue plot, which underlines our very high sensitivity to interdiffusion. The EuSe concentration profile along the growth direction for both simulations is shown as an inset in the graph. The value 1 describes a 100% occupancy of the Eu/Pb sites with Eu atoms, 0 an occupancy solely with Pb atoms. The results of all fitting parameters for each sample are summarized in Table II.

A comparison with the simulations for an x-ray energy of 8050 eV (Cu K_α radiation) in Fig. 7(b) demonstrates strik-

TABLE II. Results for the fitting procedures applied to all samples. d_{111} refers to the crystalline (111) spacing, whereas $\overline{d}$ describes the average epilayer thickness. Note that sample M1420 was fitted with a simpler model than the other samples.

Sample	M1420	M1553	M1555
d_{111}(EuSe)	3.61±0.02	3.60±0.01	3.58±0.01
$d_{111}(PbSe_{1-x}Te_x)$	3.53±0.01	3.534±0.005	3.55±0.005
$\overline{d}_{EuSe}$ (Å)	36 not fitted	47±2	46±2
$\overline{d}_{PbSe_{1-x}Te_x}$ (Å)	64 not fitted	427±4	286±4
μ (Å)	(not fitted)	1.0±0.3	1.2±0.3

ingly the resolution advantages at 2490 eV. For the same interdiffusion profiles as in (a), the two simulated diffraction curves differ significantly less. Thus the low x-ray energy is essential to achieve a sufficiently high sensitivity for the high interface quality of these structures.

V. SUMMARY

The anomalous x-ray diffraction from superstructure reflections was demonstrated to provide a unique tool for the investigation of epitaxially grown multilayers. The use of complementary wavelengths close to the absorption edges of the different constituent elements in the multilayers allows for a precise determination of both the material specific strain as well as the individual layer thicknesses. Furthermore, using low x-ray energies for the diffraction experiments results in a substantially increased sensitivity of the diffractograms for interdiffusion.

ACKNOWLEDGMENTS

We thank V. Holý for his helpful suggestions and discussions. This work was supported by the FWF, Vienna. The indispensable technical support from the staff of the beamline ID01 in Grenoble is greatly acknowledged. T. U. Schülli would like to thank the ESRF and the EC (SiGeNet) for a grant.

APPENDIX: SCATTERING THEORY USED FOR THE FITS

1. Specular kinematic diffraction from a multilayer

The scattered intensity distribution from multilayers has been studied in great detail in the last decades.[2] In this work, we refer to kinematic scattering theory, i.e., we neglect extinction of the x-ray wave by elastic scattering. This is justified, as we look at superstructure reflections which have an extinction length larger than the absorption length determined by inelastic processes. We can therefore deduce the specular reflected amplitude A as

$$A(q)=\sum_{l=1}^{N} e^{iql(M_{\mathrm{EuSe}}d_{111_{\mathrm{EuSe}}}+M_{\mathrm{PbSe}}d_{111_{\mathrm{PbSe}}})} \times\Bigg[\sum_{m_{\mathrm{PbSe}}=1}^{M_{\mathrm{PbSe}}} e^{iqm_{\mathrm{PbSe}}d_{111_{\mathrm{PbSe}}}}(f_{\mathrm{Pb}}+f_{\mathrm{Se}}e^{iq(1/2)d_{111_{\mathrm{PbSe}}}}) + e^{iqM_{\mathrm{PbSe}}d_{111_{\mathrm{PbSe}}}}\sum_{m_{\mathrm{EuSe}}=1}^{M_{\mathrm{EuSe}}} e^{iqm_{\mathrm{EuSe}}d_{111_{\mathrm{EuSe}}}} \times(f_{\mathrm{Eu}}+f_{\mathrm{Se}}e^{iq(1/2)d_{111_{\mathrm{EuSe}}}})\Bigg], \tag{A1}$$

where the first sum runs over the whole multilayer and sums up the total number of N bilayers. The phase factor in the first line of Eq. (A1) refers to the position of the bilayer l in real space. The sums in the following lines represent the atomic positions inside the PbSe film and the EuSe film, respectively. For the case of a perfect multilayer system, analytical solutions can be derived for these finite sums. However, the description in Eq. (A1) does not include absorption or any imperfection of the superlattice. One intention of this experimental work is the precise determination and hence the simulation of imperfections in these multilayers. Their inclusion in the calculation will favor the summation over all or a part of the atomic layers. Figure 8 gives an illustration on the summations and corresponding parameters. The inverse growth direction is referred to as the *positive z* direction in real space.

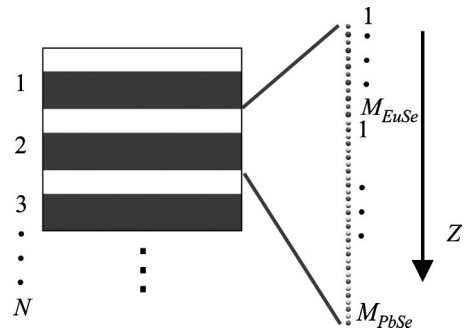

FIG. 8. Sketch of the real-space model of the superlattice and the summation indices, which run through the single films and through the multilayer.

2. Implementation of interdiffusion

Interdiffusion at the interfaces can be included in a simulation by averaging the atomic scattering factors of Eu and Pb. In the interdiffusion region, the lattice parameter and therefore the distance between the (111) planes has to be adapted accordingly. A possibility to describe such a smooth step is the function

$$c(z)=(1-e^{(-z/\nu)})^{\tau}. \tag{A2}$$

z is the spatial coordinate along the interface normal, ν and τ describe the decay. The atomic scattering factors representing Pb or Eu on the Pb/Eu lattice sites are then averaged via

$$f_{\mathrm{Eu/Pb}}=cf_{\mathrm{Eu}}+(1-c)f_{\mathrm{Pb}}. \tag{A3}$$

An equivalent expression refers to the lattice parameters. The advantage of the function (A2) is its flexibility to express an asymmetrically smoothened step with only two parameters. In Eq. (A1), this can be taken into account via a variation of the z positions in the sums concerning the PbSe and EuSe layers. The z positions for every atomic layer, which is defined by the phase factor $e^{iqm_{\mathrm{PbSe}}d_{111_{\mathrm{PbSe}}}}$ in Eq. (A1), can be changed via a variation of the atomic distances throughout one bilayer. Once the variation of the EuSe concentration throughout the bilayer is defined as sketched in the inset of Fig. 7, it can be used to calculate the average atomic scattering factor, as well as the (111) d spacing for every atomic layer. The z positions are then no longer defined by the multiplication of one value of $d_{(111)}$, but are just sums of the z position of the predecessing atomic layer and the local (111) d spacing. The latter is derived from the local composition. This changes Eq. (A1) to

$$A(q)=\sum_{k=1}^{L} e^{iqlD_{bl}} \sum_{m=1}^{M} e^{iqz(m)}(f_{\mathrm{EuPb}}(m)+f_{\mathrm{Se}}e^{iq(1/2)d_{111}(m)}) \tag{A4}$$

where the index m runs over a complete EuSe/PbSe bilayer. D_{bl} describes the total thickness of one EuSe/PbSe bilayer. The implementation of absorption and instabilities in the growth parameters for thick multilayers finally results in

$$A(q)=\sum_{k=1}^{L} e^{iqlD_{bl}(k)} \sum_{m=1}^{M(k)} A_0(k,m)e^{iqz(k,m)}(f_{\mathrm{EuPb}}(m) + f_{\mathrm{Se}}e^{iq(1/2)d_{111}(m)}) \tag{A5}$$

where $A_0(k,m)$ simulates the decay of the amplitude of the x-ray wave field caused by absorption in the multilayer.

[1] P. Zaumseil, *X-ray Diffraction Techniques*, Vol. 45, edited by R. K. Willardson and A.C. Beer, Semiconductors and Semimetals (Academic, New York, 1997), p. 261.

[2] V. Holý, U. Pietsch, and T. Baumbach, *High Resolution X-ray Diffraction from Thin Films and Multilayers*, Vol. 149, edited by G. Höhler, Springer Tracts in Modern Physics (Springer, Berlin, 1999).

[3] K.K.-W. Siu, A.Y. Nikulin, P. Zaumseil, H. Yamazaki, and T. Ishikawa, J. Appl. Phys. **94**, 1007 (2003).

[4] I.N. Goncharenko and I. Mirebeau, Phys. Rev. Lett. **80**, 1082 (1998).

[5] H. Kepa, G. Springholz, T.M. Giebultowicz, K.I. Goldman, C.F. Majkrzak, P. Kacman, J. Blinowski, S. Holl, H. Krenn, and G. Bauer, Phys. Rev. B **68**, 024419 (2003).

[6] P. Wachter, *Handbook on the Physics and Chemistry of Rare Earths*, edited by K.A. Gschneidner and L. Eyring (North-Holland, Amsterdam, 1979), p. 507.

[7] H. Kepa, J. Kutner-Pielaszek, J. Blinowski, A. Twardowski, C.F. Majkrzak, T. Story, P. Kacman, R.R. Galazka, K. Ha, H.J.M. Swagten, W.J.M. de Jonge, A.Yu. Sipatov, V. Volobuyev, and T.M. Giebultowicz, Europhys. Lett. **56**, 54 (2001).

[8] T.U. Schülli, M. Sztucki, V. Chamard, T.H. Metzger, and D. Schuh, Appl. Phys. Lett. **81**, 448 (2002).

[9] J. Baró, M. Roteta, J.M. Fernández-Varea, and F. Salvat, Radiat. Phys. Chem. **44**, 531 (1994).

[10] B.L. Henke, E.M. Gullikson, and J.C. Davis, At. Data Nucl. Data Tables **54**, 181 (1993).

[11] L. Kissel, B. Zhou, S.C. Roy, S.K. Sen Gupta, and R.H. Pratt, Acta Crystallogr., Sect. A: Found. Crystallogr. **51**, 271 (1995).

[12] See, www-phys.llnl.gov

[13] R.T. Lechner (unpublished).

[14] M. Born and E. Wolf, *Principles of Optics*, Electromagnetic Theory of Propagation, Interference and Diffraction of Light (Cambridge University Press, Cambridge, 1997).

[15] J.M. Cowley, *Diffraction Physics* (North-Holland, Amsterdam, 1981).

[16] R. Hosemann, Z. Phys. **127**, 16 (1949).

[17] D.G. Stearns, J. Appl. Phys. **65**, 491 (1989).

[18] G. Nimtz, in *Numerical Data and Functional Relationships in Science and Technology*, edited by K. Hellwege and O. Madelung, Landolt-Börnstein, New Series, Group III, Vol. 17 Pt. f (Springer-Verlag, Berlin, 1993), p. 168.

[19] D.G. Stearns, J. Appl. Phys. **71**, 4286 (1992).

[20] J.H. Li, S.C. Moss, Y. Zhang, A. Mascarenhas, L.N. Pfeiffer, K.W. West, W.K. Ge, and J. Bai, Phys. Rev. Lett. **91**, 106103 (2003).

[21] G. Springholz, V. Holy, M. Pinczolits, and G. Bauer, Science **282**, 734 (1998).